

Out-of-plane and in-plane magnetization behavior of dipolar interacting FeNi nanoislands around the percolation threshold

A. Stupakov,¹ A. V. Bagdinov,² V. V. Prokhorov,³ A. N. Bagdinova,² E. I. Demikhov,²
A. Dejneka,¹ K. I. Kugel,⁴ A. A. Gorbatshevich,² F. A. Pudonin,² and N. N. Kovaleva^{5,1,2,*}

¹*Institute of Physics ASCR, Na Slovance 2, 18221 Prague, Czech Republic*

²*Lebedev Physical Institute RAS, Leninsky prosp. 53, 119991 Moscow, Russia*

³*Frumkin Institute of Physical Chemistry and Electrochemistry RAS,
Leninsky prosp. 31, 119991 Moscow, Russia*

⁴*Institute for Theoretical and Applied Electrodynamics RAS,
Izhorskaya str. 13, 125412 Moscow, Russia*

⁵*Department of Physics, Loughborough University,
LE11 3TU Leicestershire, United Kingdom*

(Dated: October 25, 2016)

Abstract

Magnetic properties of inhomogeneous nanoisland FeNi films were studied by SQUID magnetometry. The FeNi films with nominal thickness ranging from 0.6 to 2.0 nm were deposited by rf sputtering on Sitall glass substrates and covered by a protecting Al_2O_3 layer on the top. The SQUID data indicate pronounced irreversibility behavior for the out-of-plane temperature dependent magnetization response (measured at $H \simeq 100$ Oe) using zero-field cooling (ZFC) and field cooled warming (FCW) after the applied dc magnetizing field $H_m \simeq 2$ T for the FeNi samples with the nominal thickness $1.1 \text{ nm} \lesssim d \lesssim 1.8 \text{ nm}$, below the percolation threshold. The positive difference between the FCW and ZFC data identifies two irreversibility temperature scales, $T_B \approx 50$ K and $T^* \approx 200$, which can be associated with the superparamagnetic and superferromagnetic behavior in inhomogeneous nanoisland FeNi films, respectively. However, above the film percolation threshold, we observed a crossover from the out-of-plane to in-plane magnetization orientation. Here, the in-plane FCW-ZFC difference implies negative remanent magnetization response in the temperature range $T_B \lesssim T \lesssim T^*$. The observed magnetization properties can be associated with the presence of the superferromagnetic phase in self-assembled clusters of quasi-2D metallic magnetic FeNi nanoislands.

Keywords: rf sputtered nanoisland FeNi films, dipolar magnets, superparamagnetic and superferromagnetic properties, SQUID magnetometry, zero-field-cooling (ZFC) and field cooled warming (FCW) magnetization measurements.

1. Introduction

Arrays of magnetic nanoparticles (dipolar magnets) are considered to form the basis of novel ultrahigh density magnetic data storage technology [1–3]. In dipolar magnets, each magnetic nanoparticle (NP) is in a single-domain ferromagnetic (FM) state with parallel orientation of intraparticle atomic moments arising due to strong exchange interactions. If the temperature is high enough to overcome energy barrier between different orientations of NP net magnetic moments, they exhibit the Curie-like behavior above the blocking temperature (T_B) in the so-called superparamagnetic (SPM) phase. Meanwhile, owing to strong long-range dipolar interactions, the arrays of NPs can possess magnetic ordering at comparatively high temperatures, and such regime is called superferromagnetic (SFM). Indeed, dipolar interactions of single-domain NPs comprising many atomic moments ($\sim 10^3 \div 10^5 \mu_B$) can be much stronger than ordinary dipolar interactions of localized atomic moments $\sim \mu_B$, where $\mu_B = 9.27 \cdot 10^{-21}$ emu is the Bohr magneton, which have a characteristic scale much less than 1 K. For example, one can estimate that magnetic moment m of $\text{Fe}_{21}\text{Ni}_{79}$ permalloy nanodiscs with the diameter $a \sim 10 \div 30$ nm and the height 1 nm varies from $6.8 \cdot 10^3$ to $6.1 \cdot 10^4 \mu_B$ [4]. Then, the characteristic energy of dipole-dipole interactions, $E_{dip} = \frac{2m^2}{r^3}$, of two similar single-domain nanodiscs located at the distance $r = 30$ nm varies from 2 to 180 K.

In the SFM phase, the magnetic structure in regular arrays of single-domain NPs depends essentially on the lattice type and on the particle magnetic anisotropy. The latter, in turn, strongly depends on the particle shape and size. For example, in small enough nanoplatelets, spin reorientation transition (SRT) may lead to effective perpendicular magnetic anisotropy [5]. For 2D lattices of NPs with high perpendicular anisotropy, the magnetic structure corresponds to various types of two-sublattice antiferromagnetic (AF) order. For square lattices with in-plane anisotropy, the magnetic structure has four-sublattice AF order, whereas for the triangular lattices a FM order is implemented [6]. Here, for finite fragments of triangular lattices, the ground state can be a vortex state formed by the magnetic moments lying in the plane (supervortex) [7, 8]. Similar as for soft magnetic dots [9–12], supervortex represents a topologically-nontrivial ordered state, more intricate than the standard domain structure.

Magnetic properties in quasi-2D systems of inhomogeneously distributed magnetic NPs usually exhibit complex behavior as a consequence of the SPM and SFM phase coexistence [13]. Here, local magnetic order determined by geometric self-arrangements of neighboring interacting NPs can exist. In quasi-2D systems of inhomogeneous dipolar magnets, fairly

separated weakly interacting NPs determine SPM behavior above the blocking temperature T_B , whereas strongly interacting NPs in the close-packed assemblies are responsible for SFM behavior. By using electron holography with sub-particle resolution, local in-plane FM vs. AF order was observed in assemblies of ~ 15 nm Co nanoparticles, depending on the close-packed triangular vs. square arrangements, and even several flux-closed regions, which can be associated with a supervortex state, were recognized [14]. These results are supported by the numerical simulations, which emphasize that local dipolar magnetism in quasi-2D inhomogeneous NP systems survives even at a pronounced structural disorder [14].

Here, by using SQUID magnetometry, we study in-plane and out-of-plane magnetic response in inhomogeneous nanoisland FeNi films, composed of flat nanoislands with lateral sizes of $5 \div 30$ nm, with the nominal film thickness varying from 0.6 to 2.0 nm (as schematically illustrated by Fig. 1). The inhomogeneous FeNi films were grown by rf sputtering deposition on Sitall glass substrates, commonly used as film substrates in microelectronics. The experimental notice presented in Ref. [15], where equatorial magneto-optical Kerr effect was studied in periodic structures of alternating FeNi and Co nanoisland layers, suggests that a supervortex collective state is essentially relevant here. We present the evidence of the out-of-plane SFM magnetization behavior for the FeNi films with the nominal film thickness $1.1 \text{ nm} \lesssim d \lesssim 1.8 \text{ nm}$, below the physical percolation threshold. Recently, the out-of-plane SFM behavior in quasi-2D Fe(2.5 nm)/Al₂O₃ multilayer composites was reported [13]. Moreover, we found a crossover from the out-of-plane to in-plane magnetization orientation with increasing nominal FeNi film thickness across the physical percolation threshold and discovered negative remanent magnetization response. This is in agreement with the earlier observation of negative remanence in nearly percolating magnetic granular (Ni,Fe) films in an insulating amorphous SiO₂ matrix by Yan *et al.* [16]. The understanding of the found out-of-plane and in-plane magnetization properties, associated with self-organized ensembles of quasi-2D single-domain FM FeNi nanoislands is quite important for the fundamental physics of magnetism, as well as for technological applications.

2. Materials and Methods

2.1. FeNi films growth and characterization

The nanoisland FeNi films were grown by rf sputtering deposition from Fe₂₁Ni₇₉ targets at a base vacuum pressure less than 2×10^{-6} Torr and a background argon pressure of 4×10^{-4}

Torr. Glass-like Sitall material was used for substrates. The analysis of an X-ray diffraction pattern of the used Sitall substrate showed that it is represented by TiO_2 rutile phase [17]. During the deposition, the substrate temperature was $73 \pm 3^\circ\text{C}$. The nominal film thickness (that is, the thickness of the corresponding continuous film) was controlled by the deposition rate and time (see more details in Ref. [18]). We prepared the nanoisland FeNi films with nominal thickness varying from 0.6 to 2.0 nm. Our earlier spectroscopic ellipsometry studies of the nanoisland FeNi films of different thickness grown on the Sitall glass demonstrated that their dielectric permittivity changes from insulating- to metallic-like at the nominal FeNi film thickness about 1.8 nm. In addition, the temperature dependence of dc conductivity suggests the existence of the percolation threshold for the same nominal FeNi film thickness [19]. To avoid oxidation of the films at ambient conditions, the grown FeNi films were covered *in situ* by the Al_2O_3 capping layer 2.1 nm thick.

2.2. Atomic-force microscopy study of the grown FeNi films

Surface morphology of the nanoisland FeNi films grown by the rf sputtering deposition on the Sitall glass substrates was studied by atomic-force microscopy (AFM) using Ntegra Prima (NT-MDT, Zelenograd, Russia) facility. Figure 2(a) represents a large-scale AFM image of the FeNi film sample [Al_2O_3 (2.1 nm)/FeNi (d)/Sitall substrate] with the nominal film thickness $d \simeq 1.2$ nm. The shown large-scale topography profile indicates the height variation in the range $1 \div 3$ nm, which characterizes the surface roughness. The smaller-size image in Fig. 2(b) clearly identifies the grainy structure with the grain lateral dimensions in the range of $15 \div 25$ nm. Due to intrinsically uneven surface of the substrate, the grain height fluctuates strongly. The typical height is of about 1 nm [see the height profile in Fig. 2(b)]. The inevitable AFM broadening does not allow estimating the real width of gaps between the grains. Figure 2(c) represents an AFM image of the FeNi film sample [Al_2O_3 (2.1 nm)/FeNi (d)/Sitall substrate] with the nominal film thickness $d \simeq 1.9$ nm. Due to appreciable coalescence of the nanoislands in the film with the thickness above the percolation threshold at $d_c \simeq 1.8$ nm [19] the topography profile is more shallow in the percolating regions.

2.3. SQUID measurements

For magnetization measurements, we cut out the FeNi film samples of approximate dimen-

sions $3 \times 3 \text{ mm}^2$. Using the SQUID magnetometer MPMS XL 7 T, we were able to measure magnetization in the temperature range from 2 to 300 K. High sensitivity of magnetic measurements ($2 \times 10^{-8} \text{ emu}$) was enabled by reciprocating sample transport. Recently by using a MPMS XL 7 T SQUID magnetometer total magnetization of d^0 charge-imbalanced FM interface between nonmagnetic perovskites of the order of 10^{-6} emu was reported [20]. For the zero-field-cooled (ZFC) measurements, a sample was first cooled down to $T \simeq 5 \text{ K}$ in zero magnetic field. Then, the magnetic field $H \simeq 100 \text{ Oe}$ was applied, and the ZFC data were collected, while the sample is slowly warmed up above the irreversibility temperature. We would like to point out that for single-domain $\text{Fe}_{21}\text{Ni}_{79}$ nanoislands, the stray magnetic fields at the edge constitute 1.08 T. Therefore, to avoid uncertainties in the determination of the equilibrium magnetization at small H and to achieve a fully polarized magnetic state, we applied the large magnetizing field $H_m \simeq 2 \text{ T}$, while the film sample was cooled down to 5 K, and finally switching the field off. Then, the field cooled warming (FCW) data were collected, while the sample is slowly warmed up in the same measurement field $H \simeq 100 \text{ Oe}$. In a more usual protocol, after the ZFC part, a second set of data is collected while the sample is slowly cooled down in the same field, the field-cooled (FC) part. However, use of the ZFC-FC protocol, when the measurement field is not large, usually of about $100 \div 200 \text{ Oe}$, cannot guarantee a fully polarized magnetic state in our case.

3. Results and Discussion

Figure 3(a-d) shows the ZFC and FCW magnetization response of the FeNi film samples (schematically illustrated by Fig. 1) with different nominal film thickness varying from 0.61 to 2.04 nm, registered in the in-plane and out-of-plane geometry of the applied magnetic field. To compare the ZFC and FCW magnetization response, $M_0(T)$, measured for the different FeNi film samples, the magnetization response was normalized to the equal sample area, $S = 10^{-1} \text{ cm}^2$ (which is typical for our samples measured here by SQUID magnetometry), using the following formula

$$M_0^{norm}(T) \simeq S \rho_S L \frac{M_0(T)}{m_0}, \quad (1)$$

where m_0 is the sample mass, $\rho_S \simeq 2.72 \pm 0.08 \text{ g/cm}^3$ is the Sitall substrate density, and $L \simeq 0.056 \pm 0.004 \text{ cm}$ is the substrate thickness. The normalized magnetization response of the FeNi film samples shown in Fig. 3(a-d) is typical paramagnetic-like, due to the

dominating contribution of the Si(111) substrate, which contains clustered magnetic impurities and/or defects [21].

One can notice that the out-of-plane magnetization response, $M_0^{norm}(T)$, clearly demonstrates difference between the FCW and ZFC curves for all studied samples [see the top panels of Fig. 3(a-d)]. However, we found that the FCW-ZFC difference is remarkably pronounced for the FeNi film samples with the nominal film thickness $1.1 \text{ nm} \lesssim d \lesssim 1.8 \text{ nm}$, where the associated irreversibility behavior persisted up to $T^* \approx 200 \text{ K}$ [see Figs. 3(b-d) and 4(b)]. In addition, a clear kink was observed there for the out-of-plane FCW-ZFC difference at $T_B \approx 50 \text{ K}$ [as illustrated by Fig. 4(b)]. The revealed temperatures, $T_B \approx 50 \text{ K}$ and $T^* \approx 200 \text{ K}$, indicate the existence of two different temperature scales for the out-of-plane irreversibility behavior of the studied nanoisland FeNi films. We noticed an apparent analogy to the results for the quasi-2D Fe(2.5 nm)/Al₂O₃ multilayer composites at low-filling factor [13]. In line with Ref. [13], the temperatures $T_B \approx 50 \text{ K}$ and $T^* \approx 200 \text{ K}$ can be associated with the SPM and SFM behavior, respectively. Here, fairly separated and weakly interacting small FeNi nanoislands determine the SPM behavior above the blocking temperature $T_B \approx 50 \text{ K}$, whereas strongly interacting FeNi nanoislands in their dispersive assemblies are responsible for the induced out-of-plane SFM behavior. The latter is indicated by the additional hysteretic-like contribution persistent up to the higher irreversibility temperature $T^* \approx 200 \text{ K}$ [as it is schematically illustrated by Fig. 5(b)]. From Fig. 4(b) one can estimate that the SFM hysteretic-like contribution attains its maximum of about $1.8 \cdot 10^{-6} \text{ emu}$ at low temperatures ($\approx 20 \%$ from the saturation magnetization of Fe₂₁Ni₇₉ permalloy [4], here one should take into account that saturation magnetization of NPs is usually somewhat less than that of a bulk material).

Analyzing the in-plane normalized magnetization response, $M_0^{norm}(T)$, obtained from the FCW and ZFC measurements, we can distinguish three different types of behavior, depending on the nominal FeNi film thickness [see the bottom panels of Fig. 3(a-d) and Fig. 4(a-c)]. Thus, for the thinnest investigated FeNi film sample (i) with the nominal thickness $d \simeq 0.61 \text{ nm}$, the FCW-ZFC difference is quite small [see Fig. 3(a)]. Here, the in-plane FCW-ZFC difference starts to deviate from nearly zero values (within the experimental accuracy) below $\approx 60 \div 70 \text{ K}$ [see Fig. 4(a)], indicating the associated SPM character of the irreversibility behavior below the blocking temperature [as it is schematically demonstrated by Fig. 5(a)]. The normalized FCW-ZFC difference attains its maximum of about $2 \cdot 10^{-6} \text{ emu}$

at 5 K ($\approx 45\%$ from the saturation magnetization of $\text{Fe}_{21}\text{Ni}_{79}$ permalloy [4]) [see Fig. 4(a)].

However, for the studied FeNi film samples (ii) with nominal thickness in the range $1.1\text{ nm} \lesssim d \lesssim 1.8\text{ nm}$, the in-plane response did not show clearly perceptible difference between the temperature dependent magnetization response using ZFC and FCW at the dc magnetizing field $H_m \simeq 2\text{ T}$ [see Figs. 3(b,c) and 4(b)].

And finally, there is a remarkable difference between the in-plane FCW and ZFC normalized magnetization curves for the FeNi film sample (iii) with the thickness $d \simeq 2.04\text{ nm}$, above the physical percolation threshold at $d_c \simeq 1.8\text{ nm}$ [19] [see the bottom panel of Fig. 3(d)]. Here, the in-plane ZFC curve shows a pronounced maximum at the blocking temperature $T_B^c \simeq 25\text{ K}$. This implies the existence of a crossover from the out-of-plane to in-plane magnetization orientation. The $T_B^c \simeq 25\text{ K}$ seemingly manifests SPM properties in the FeNi film close to the percolation threshold at $d_c \simeq 1.8\text{ nm}$ [19]. Below T_B^c , the normalized FCW-ZFC difference attains its maximum of about $6 \cdot 10^{-6}\text{ emu}$ at 10 K ($\approx 37\%$ from the saturation magnetization of $\text{Fe}_{21}\text{Ni}_{79}$ permalloy [4]) [see Fig. 4(c)]. Surprisingly, here the in-plane FCW curve exhibits lower magnetization values than that of the corresponding ZFC curve from about T_B^c to $T^* \approx 200\text{ K}$ [see the bottom panel of Fig. 3(d)]. Due to this, the normalized FCW-ZFC difference turns out to be negative, with a pronounced minimum of about $-1.8 \cdot 10^{-6}\text{ emu}$ around 50 K [see Fig. 4(c)]. And, with rising temperature above the SFM irreversibility temperature $T^* \approx 200\text{ K}$, the FCW-ZFC difference vanishes. In contrast to the induced out-of-plane SFM behavior found below the percolation threshold, where the FCW curve lies above the ZFC curve, here the FCW curve lies below the ZFC curve. According to our simple modeling, this behavior can be adjusted by the negative SFM contribution [as it is schematically illustrated by Fig. 5(c)]. The found behavior indicates that the magnetization response is in a direction opposite to the applied dc magnetizing field $H_m \simeq 2\text{ T}$ (while the film sample was cooled down from above $T^* \approx 200\text{ K}$ to 5 K), and can be associated with the SFM component.

Figure 6(a,b) displays temperature dependence of the in-plane and out-of-plane normalized remanent magnetization response of the nanoisland FeNi film samples [capping Al_2O_3 layer (2.1 nm)/FeNi film (d)/Sitall substrate] produced by the magnetizing field $H_m \simeq 1\text{ T}$ at 10 K . Here, after the magnetizing field was switched off, the remanent magnetization was recorded at zero external magnetic field ($H \simeq 0\text{ T}$) on rising temperature from 10 to 300 K , and then on cooling down to the lowest measuring temperature. The magnetization mea-

surements at $H \simeq 0$ T allowed us to get rid of the paramagnetic-like contribution of the Si substrate [dominating the magnetization response shown in Fig. 3(a-d)]. One can notice from Fig. 6(a) that the out-of-plane remanent magnetization of the FeNi film with the thickness $d \simeq 1.1$ nm decreases from about $5 \cdot 10^{-6}$ emu at 10 K ($\approx 57\%$ from the saturation magnetization of Fe₂₁Ni₇₉ permalloy [4]) to about $2 \cdot 10^{-6}$ emu at 300 K ($\approx 23\%$, respectively). The observed trends of the in-plane remanent magnetization are the most pronounced for the FeNi film sample with the nominal thickness $d \simeq 2.04$ nm [see Fig. 6(b)]. Here, the FeNi film was initially magnetized along the magnetic field ($H_m \simeq 1$ T) direction applied in the film plane at 10 K. Surprisingly, with rising temperature up to 50 K, the in-plane normalized remanent magnetization relaxed down to negative values of about $-2 \cdot 10^{-6}$ emu. Here, above the blocking temperature T_B , large magnetic moments of individual SPM nanoislands become strongly fluctuating, and the resulting contribution from the SPM component is zero at $H \simeq 0$. This means that some parts of the FeNi film, related to the SFM component, retain the magnetization opposite to the applied magnetizing field $H_m \simeq 1$ T. Indeed, with further increasing temperature above the irreversibility temperature T^* , the negative magnetization response disappeared, and the in-plane remanent magnetization attained a small value at 300 K. Interestingly, the in-plane temperature dependence of the magnetization was reproducible at subsequent cooling down, exhibiting the same negative magnetization response below 150 K down to 50 K. This means that the negative magnetization component is related to a magnetically-ordered ground state of the SFM phase. It remains intact to the applied magnetizing field $H_m \simeq 1$ T, preserving the initial magnetization orientation. The result shown in Fig. 6(b) suggests that around 50 K the inverted hysteresis $M - H$ loop will be observed for the in-plane measurements, with the negative magnetization value of -12% at $H \simeq 0$ (normalized to positively saturated value). One can notice from Fig. 6(a) that the temperature dependence of the in-plane remanent magnetization of the FeNi film with the nominal thickness $d \simeq 1.1$ nm showed, in main, similar trends. However, the observed temperature effects were less pronounced here and shifted to lower temperatures. We note that the observed trends of the remanent magnetization have a strong resemblance to the results of the independent FCW-ZFC measurements [see Fig. 4(b,c)], giving supporting experimental evidence.

Now we discuss the observed magnetization properties. The observed out-of-plane SFM behavior below the percolation threshold can be associated with an effective perpendicular

magnetic anisotropy in the rf sputtered FeNi films composed of quasi-2D FM FeNi nanoislands. For example, an effective perpendicular anisotropy can exist in small enough quasi-2D FeNi nanoislands due to SRT [5]. As a result, the local magnetic structure may correspond to AF ground state on square or triangular lattice fragments of self-assembled quasi-2D FeNi nanoislands. In addition, here we observed a crossover from the out-of-plane to in-plane magnetization orientation with increasing the nanoisland size close to the percolation transition. Here, the in-plane magnetic structure may have four-sublattice AF order for square lattice fragments, whereas a FM order may be implemented for the triangular lattice fragments.

We would like to note that such system with an effective perpendicular magnetic anisotropy has also a tendency to inhomogeneous distribution of magnetic moments in the form of supervortices [8]. We infer that the studied nanoisland FeNi films, composed of inhomogeneously distributed FM single-domain nanoislands, represent a unique playground to challenge a supervortex state and its magnetic properties. For small magnetic anisotropy, a purely planar vortex can exist on close-packed hexagonal fragments of a triangular lattice, with in-plane distribution of FM NP's magnetic moments. Here, the total out-of-plane projection of the magnetic moment vanishes, but the in-plane component of the total magnetization is nonzero, as the magnetic moment of the vortex core remains not compensated [8]. This may be relevant to the in-plane magnetization properties found in the present study for the nanoisland FeNi film with the nominal film thickness above the percolation threshold at $d_c \simeq 1.8$ nm. With the increase of the particle magnetic anisotropy, the vortex core starts to protrude out-of-plane. And with the further increase, the symmetry of the vortex ground state increases, where the planar magnetization component vanishes (featuring zero-net magnetic moment), but the perpendicular component changes significantly [8]. This may be well consistent with the magnetization properties found in the present study for the nanoisland FeNi films with the nominal film thickness $1.1 \text{ nm} \lesssim d \lesssim 1.8 \text{ nm}$.

Recently the out-of-plane SFM behavior in quasi-2D Fe(2.5 nm)/Al₂O₃ multilayer composites was reported [13]. The results by Miu *et al.* indicate that the dipolar interactions are not the major interactions and support the relevance of two-dimensionality and additional short-range “superexchange” interactions for the occurrence of the out-of-plane SFM behavior in quasi-2D FM NPs above some critical filling factor (see Ref. [13] and references therein). In particular, the stray fields of non-point-like magnetic dipoles can promote

this “superexchange” and drive SFM order in quasi-2D FM NPs. In addition, an indirect Ruderman-Kittel-Kasuya-Yosida (RKKY) interaction between FM NPs in quasi-2D magnetic structures can contribute to the short-range “superexchange” coupling mechanism and be responsible for SFM behavior [22]. Thus, the SFM phase, associated with complex magnetic behavior in quasi-2D clusters of large NP’s localized magnetic moments implies essentially a Many-Body Localized (MBL) state [23].

In addition, here we demonstrated that the discovered in-plane negative magnetization response above the nanoisland FeNi film percolation threshold can be associated with the SFM component. Earlier, negative remanent magnetization was observed in nearly percolating magnetic granular (Ni,Fe) films in an insulating amorphous SiO₂ matrix [16]. The temperature dependent remanence magnetization observed there and shown in Fig.2 of Ref.[16] is similar to the in-plane magnetization behavior found in the present study for FeNi nanoislands above the percolation threshold [see Figs.4(c) and 6(b)]. The remanence observed in Ref.[16] was as large as -9% compared to the positively saturated value. It was suggested in this study that near the percolation threshold the magnetostatic interaction between coexisting SPM and FM components, with a special geometry of the FM nanoclusters, favors their opposite alignment, induced by the applied magnetizing field. An alternative interpretation in terms of interface exchange interaction or exchange anisotropy was suggested for similar phenomena observed in amorphous and multilayered materials (see Ref.[16] and references therein). The negative remanent magnetization is possible in an exchange-coupled bilayer, when a magnetically soft material is influenced by the demagnetizing field of the hard material. However, all these has a strong similarity with exchange bias effect, actively studied in many composite magnetic materials.

4. Conclusions

We present the evidence of the out-of-plane SFM behavior for the nanoisland FeNi films with the nominal film thickness $1.1\text{ nm} \lesssim d \lesssim 1.8\text{ nm}$ below the percolation threshold at $d_c \simeq 1.8\text{ nm}$ [19] in the temperature range, which fits well to the estimated characteristic energy of the long-range dipolar interactions of about 180 K (the estimate is given in the Introduction). The SFM behavior is indicated by the additional hysteretic-like contribution persistent up to the irreversibility temperature $T^* \approx 200\text{ K}$. Besides, an admixture of the SPM phase was identified here by a clear kink in the out-of-plane FCW-ZFC difference at $T_B \simeq 50\text{ K}$.

Above the film percolation threshold, we observed a crossover from the out-of-plane to in-plane magnetization orientation. Here, the ZFC curve shows a clear maximum near the blocking temperature $T_B^c \simeq 25$ K, which certifies the presence of SPM component. The in-plane FC-ZFC difference turns out to be negative in the temperature range $T_B \lesssim T \lesssim T^*$, implying that the magnetization response is in a direction opposite to the applied dc magnetizing field $H \simeq 2$ T. The investigation of $M(H)$ hysteresis loops at small applied magnetic fields at different temperatures will be interesting and relevant here. We showed that the discovered in-plane negative magnetization response above the nanoisland FeNi film percolation threshold can be associated with the SFM component. From our study, we can conclude that the negative magnetization response can be related to some parts of the FeNi film, which retain the magnetization opposite to the applied magnetizing field, preserving their initial magnetization orientation. These parts, related to the SFM component, can be considered as being magnetically hard, so that the direction of their magnetization could not be changed by the applied magnetizing field. The origin of the magnetically hard component in the studied nanoisland FeNi films needs to be further investigated. For example, its relevance to a core of the purely planar vortex, which can exist on close-packed hexagonal fragments of a triangular lattice here, with in-plane distribution of FM NP's magnetic moments, should be challenged.

We conclude that the observed magnetization properties can be associated with the SFM behavior in self-assembled clusters of quasi-2D metallic magnetic FeNi nanoislands. The SFM phase, associated with complex magnetic behavior in quasi-2D clusters of large NP's localized magnetic moments ($\sim 10^3 \div 10^5 \mu_B$) implies a MBL state. The electronic excitations [23–25] of this MBL state and response to strong applied magnetic fields need to be further fundamentally studied. Also, the understanding of the found out-of-plane and in-plane SFM behavior, associated with self-organized ensembles of quasi-2D single-domain nanoislands, requires further studies by using, for example, magnetic imaging techniques.

Abbreviations

ZFC: zero-field cooling, FC: field cooling, FCW: field-cooled warming, NP: nanoparticle, FM: ferromagnetic, SPM: superparamagnetic, SFM: superferromagnetic, SRT: spin reorientation transition, AF: antiferromagnetic, AFM: atomic-force microscopy.

Conflict of Interests

The authors declare no competing financial interests.

Acknowledgments

The authors acknowledge fruitful discussions with M. Forrester, F. Kusmartsev, and N. Sibeldin. This work was supported by the Czech Science Foundation GA CR (Grant No. 15-13778S) and by the Russian Foundation for Basic Research (projects 14-02-00276 and 16-02-00304). Our experiments were performed in MLTL (<http://mltl.eu>), which is supported within the program of Czech Research Infrastructures (project no. LM2011025).

References

-
- * Electronic address: N.Kovaleva@lboro.ac.uk
- [1] S. Sun and C. B. Murray, “Synthesis of monodisperse cobalt nanocrystals and their assembly into magnetic superlattices,” *Journal of Applied Physics*, vol. 85, no. 8, pp. 4325–4330, 1999.
 - [2] G. Reiss and A. Hütten, “Applications beyond data storage,” *Nature Materials*, vol. 4, no. 10, pp. 725–726, 2005.
 - [3] N. A. Frey and S. Sun, “Magnetic Nanoparticle for Information Storage Applications. Inorganic Nanoparticles: Synthesis, Applications, and Perspectives,” *CRC Press*, 2011.
 - [4] Here the saturation magnetization $M_S \simeq 800 \text{ emu/cm}^3$.
 - [5] E. Y. Vedmedenko, H. P. Oepen, and J. Kirschner, “Size-dependent spin reorientation transition in nanoplatelets,” *Physical Review B*, vol. 67, no. 1, pp. 012409–1–4, 2003.
 - [6] V. M. Rozenbaum, V. M. Ogenko and A. A. Chuiko, “Vibrational and orientational states of surface atomic groups,” *Soviet Physics Uspekhi*, vol. 34, no. 10, pp. 883-902, 1991.
 - [7] P. Politi, M. G. Pini and R. L. Stamps, “Dipolar ground state of planar spins on triangular lattices,” *Physical Review B*, vol. 73, no. 2, pp. 020405(R)–1–4, 2006.
 - [8] S. A. Dzian, A. Yu. Galkin, B. A. Ivanov et al., “Vortex ground state for small arrays of magnetic particles with dipole coupling,” *Physical Review B*, vol. 87, no. 18, pp. 184404-1-184404-6, 2013.

- [9] M.-Y. Im, P. Fischer, K. Yamada et al., “Symmetry breaking in the formation of magnetic vortex states in a permalloy nanodisk,” *Nature Communications*, vol. 3, pp. 983–988, 2012.
- [10] R. P. Cowburn, D. K. Koltsov, A. O. Adeyeye et al., “Single-domain circular nanomagnets,” *Physical Review Letters*, vol. 83, no. 5, pp. 1042–1045, 1999.
- [11] T. Shinjo, T. Okuno, R. Hassdorf et al., “Magnetic vortex core observation in circular dots of permalloy,” *Science*, vol. 289, no. 5481, pp. 930–932, 2000.
- [12] A. Wachowiak, J. Wiebe, M. Bode et al., “Direct observation of internal spin structure of magnetic vortex cores,” *Science*, vol. 298, no. 5593, pp. 577–580, 2002.
- [13] D. Miu, S. I. Jinga, B. S. Vasile et al., “Out of plane superferromagnetic behavior of quasi two-dimensional Fe/Al₂O₃ multilayer nanocomposites,” *Applied Physics Letters*, vol. 117, no. 7, pp. 074303–1–4, 2015.
- [14] M. Varón, M. Beleggia, T. Kasama et al., “Dipolar magnetism in ordered and disordered low-dimensional nanoparticle assemblies,” *Scientific Reports* vol. 3, pp. 1234–1–5, 2013.
- [15] A. P. Boltaev, F. A. Pudonin, and I. A. Sherstnev, “Vortex-like magnetization of multilayer magnetic nanoisland systems in weak magnetic fields,” *Applied Physics Letters*, vol. 102, no. 14, pp. 142404–1–3, 2013.
- [16] X. Yan and Y. Xu, “Negative remanence in magnetic nanostructures,” *Journal of Applied Physics*, vol. 79, no. 8, pp. 6013–6015, 1996.
- [17] N. N. Kovaleva, D. Chvostova, A. V. Bagdinov et al., “Interplay of electron correlations and localization in disordered β -tantalum films: Evidence from dc transport and spectroscopic ellipsometry study,” *Applied Physics Letters*, vol. 106, no. pp. 051907–1–5, 2015.
- [18] A. P. Boltaev, F. A. Pudonin, I. A. Sherstnev, “Specific features of the magnetoresistance in multilayer systems of magnetic nanoislands in weak magnetic fields,” *Physics of the Solid State*, vol. 53, no. 5, pp. 950–956, 2011.
- [19] I. A. Sherstnev, PhD thesis “Electronic transport and magnetic structure of nanosland ferromagnetic materials systems”, <http://www.lebedev.ru/ru/dissertation-councils/vak.html?date=2014-04-28>.
- [20] R. Oja, M. Tyunina, L. Yao et al., “Ferromagnetic interface between nonmagnetic perovskites,” *Physical Review Letters*, vol. 109, no. 12, pp. 127207–1–5, 2012.
- [21] We fitted the in-plane magnetization field dependence of the Sitall substrate measured at

- $T \simeq 10$ K with the Langevin function $M(H, T) = N_p \mu_p \left[\coth \left(\frac{\mu_p H}{k_B T} \right) - \frac{k_B T}{\mu_p H} \right]$, where k_B is the Boltzmann's constant, and estimated average magnetic moment of magnetic impurities $\mu_p \simeq 6\mu_B$ and their concentration $N_p \simeq 2.03 \cdot 10^{19} \text{ cm}^{-3}$.
- [22] J. Du, B. Zhang, R. K. Zheng et al., "Memory effect and spin-glass-like behavior in Co-Ag granular films," *Physical Review B*, vol. 75, no. 1, pp. 014415–1–7, 2007.
 - [23] N. N. Kovaleva, K. I. Kugel, A. V. Bazhenov et al., "Formation of metallic magnetic clusters in a Kondo-lattice metal: Evidence from an optical study," *Scientific Reports*, vol. 2, pp. 890–1–7, 2012.
 - [24] N. N. Kovaleva, A. V. Boris, C. Bernhard et al., "Spin-controlled Mott-Hubbard bands in LaMnO_3 probed by optical ellipsometry," *Physical Review Letters*, vol. 93, no. 14, pp. 147204–1–4, 2004.
 - [25] N. N. Kovaleva, A. V. Boris, P. Yordanov et al., "Optical response of ferromagnetic YTiO_3 studied by spectral ellipsometry," *Physical Review B*, vol. 76, no. 15, pp. 155125–1–11, 2007.

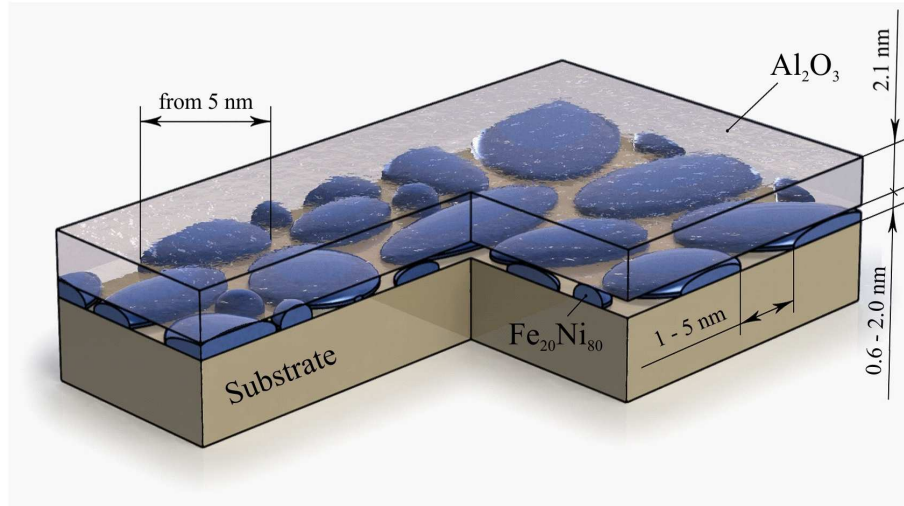


FIG. 1: A schematic picture of the nanoisland FeNi film samples [capping Al_2O_3 layer (2.1 nm)/FeNi (d)/Sital substrate].

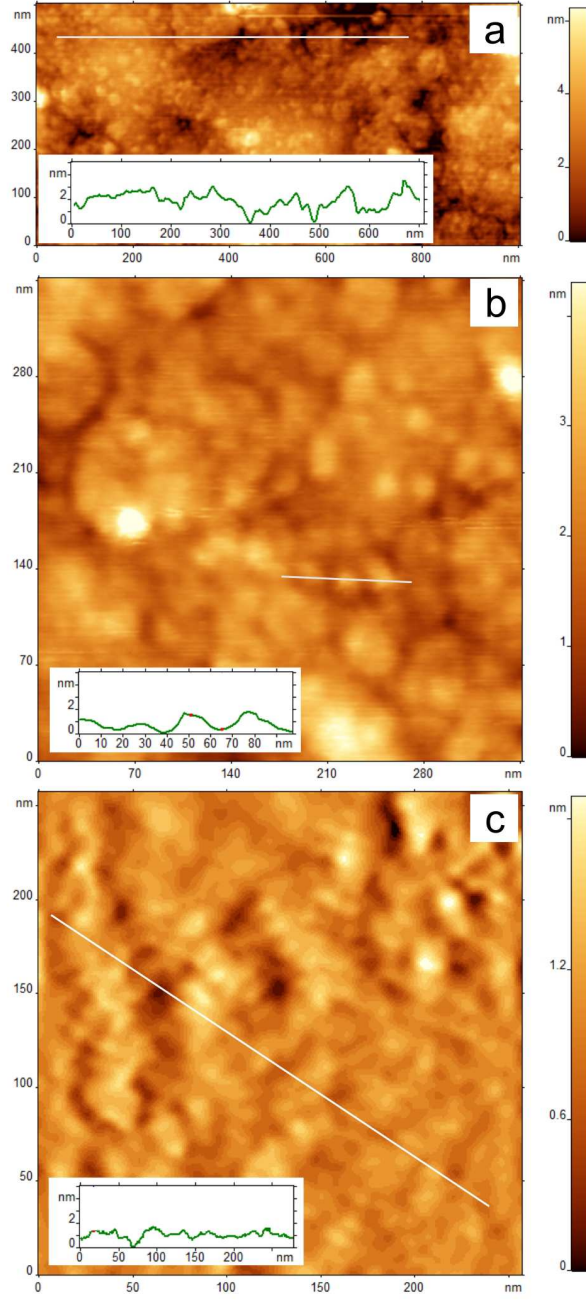


FIG. 2: AFM images of the FeNi film samples $[\text{Al}_2\text{O}_3 (2.1 \text{ nm})/\text{FeNi} (d)/\text{Sital substrate}]$ with the nominal film thickness (a,b) $d \simeq 1.2 \text{ nm}$ and (c) $d \simeq 1.9 \text{ nm}$.

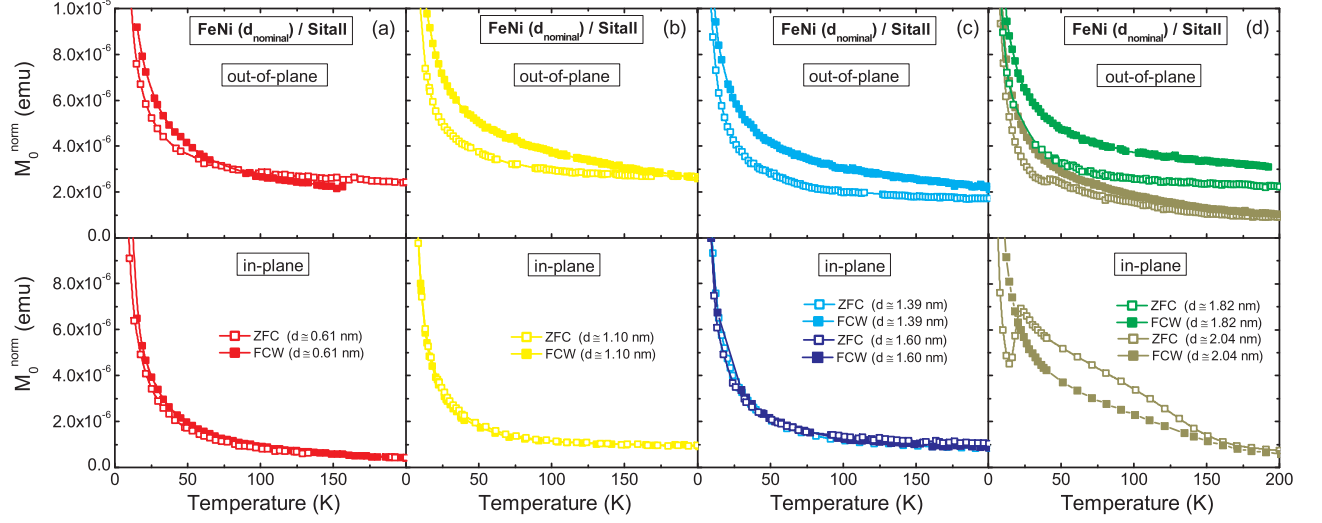


FIG. 3: The out-of-plane (top panels) and in-plane (bottom panels) ZFC and FCW normalized magnetization response [calculated using Eq.(1)] of the nanoisland FeNi film samples $[\text{Al}_2\text{O}_3 (2.1 \text{ nm})/\text{FeNi}(d)/\text{Si(111)}]$ with the nominal film thickness of (a) 0.61 nm, (b) 1.10 nm, (c) 1.39 and 1.60 nm, and (d) 1.82 and 2.04 nm. The displayed symbols are larger than the error bars. The solid curves are the guides to the eye.

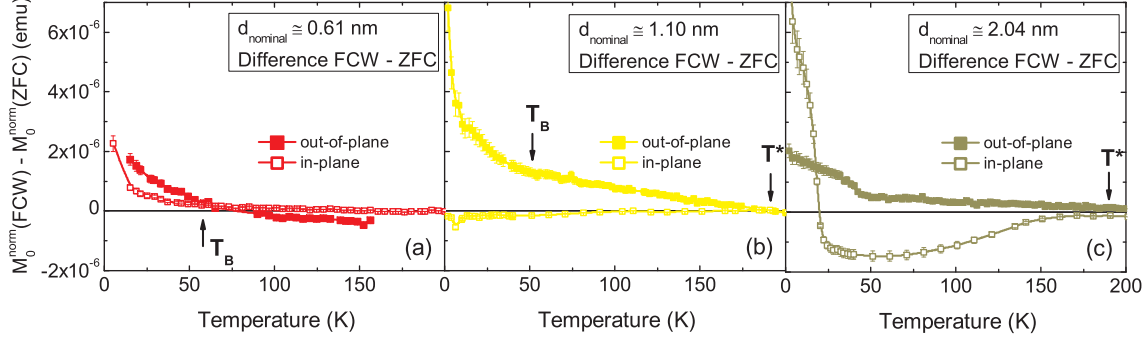


FIG. 4: The difference between the FCW and ZFC normalized magnetization response shown in Fig.3 for the FeNi film samples $[\text{Al}_2\text{O}_3 (2.1 \text{ nm})/\text{FeNi} (d)/\text{SiAl}$ substrate] with the nominal film thickness (a) 0.61 nm, (b) 1.10 nm, and (c) 2.04 nm in the out-of-plane and in-plane sample configuration. The solid curves are the guides to the eye.

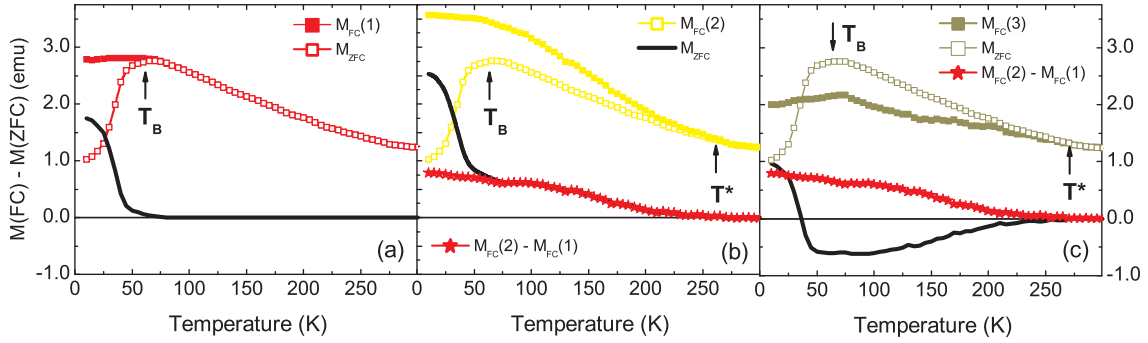


FIG. 5: A schematic illustration of the temperature-dependent ZFC and FC magnetization response (and of the associated difference) for FM NPs. (a) For SPM phase of weakly interacting NPs. (b) For SPM phase of weakly interacting NPs, coexisting with SFM phase of strongly interacting NPs. Here red star symbols correspond to the additional hysteretic-like SFM contribution. (c) Modeling the in-plane negative response [shown in Fig. 4(c)] above the NP's system percolation threshold. Here the FC curve is obtained by subtraction of the SFM contribution.

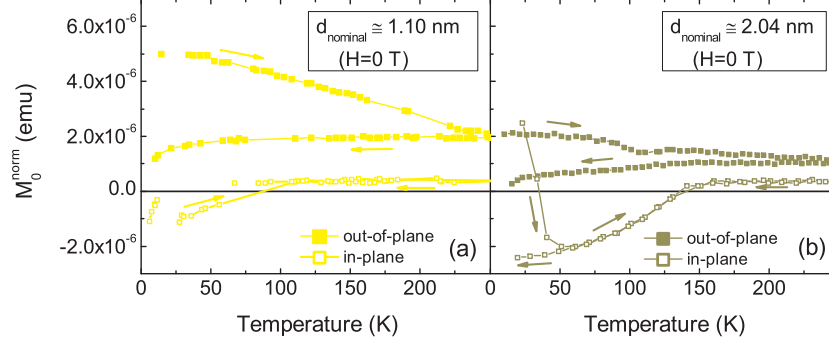


FIG. 6: The temperature dependence of the normalized remanent magnetization, produced by the in-plane and out-of-plane magnetizing field $H_m \simeq 1\text{T}$ at $T \simeq 10\text{ K}$ in the studied FeNi film samples $[\text{Al}_2\text{O}_3 (2.1\text{ nm})/\text{FeNi} (d)/\text{Si}/\text{tall substrate}]$ with the nominal film thickness (a) 1.10 nm and (b) 2.04 nm. Arrows indicate the magnetization response ($H \simeq 0$) with cycling temperature from 10 K to 300 K and back, down to low temperatures. The displayed symbols are larger than the error bars. The solid curves are the guides to the eye.